International Journal of Thermophysics, Vol. 18, No. 3, 1997

Thermal Diffusivity of the Alternative Refrigerant R152a

B. Kruppa[1,2] **and J. Straub**[3]

Received August 8, 1996

The thermal diffusivity of R152a was measured by dynamic light scattering. We have developed an apparatus which enables us to apply both homodyne and heterodyne light-scattering techniques allowing a wide region of state to be investigated. A total of 300 data points was obtained along the critical isochore, in both coexisting phases and on seven isotherms with densities and temperatures ranging from 50 to 1000 $kg \cdot m^{-3}$ and 290 to 425 K, respectively. The uncertainty of the measurements lies between 0.5 and 5%. The thermal-diffusivity values cover a range of over four orders of magnitude and include the region around the vapor–liquid critical point. Other measured properties are temperature, pressure, and refractive index as well as the critical parameters T_c and p_c.

KEY WORDS: critical region; light scattering; refrigerants; R152a; thermal diffusivity; transport properties.

1. INTRODUCTION

The ozone depletion potential (ODP) and the total equivalent warming impact (TEWI) are two important factors which determine whether a substance can qualify as a suitable alternative refrigerant. Other requirements are inflammability, low toxicity, chemical stability, favorable thermodynamic properties, and compatibility with lubricant oils. While an ODP of zero can be satisfied, as is the case with the halogenated HFC's R152a,

[1] Bundesindustrieverband Heizungs-, Klima-, Sanitärtechnik e. V., Weberstrasse 33, 53113 Bonn, Germany.

[2] To whom correspondence should be addressed.

[3] Lehrstuhl A für Thermodynamik, Technische Universität München, P.O. Box 202420, 80333 München, Germany.

0195-928X/97/0500-0807$12.50/0

R32, R134a, R125, R143a, and R227, the TEWI or global warming potential (GWP) of these substances varies considerably. From the above group, R152a has the lowest global warming potential (GWP = 0.03) and would otherwise seem an ideal choice, were it not for its flammability. In the current search for a long-term replacement of the refrigerants R22 and R502, R152a is an interesting candidate as a component in binary or ternary mixtures. Thermophysical-property data, in particular transport-property data, of R152a are scarce; the thermal diffusivity of R152a has, to our knowledge, not yet been investigated systematically. For calculations involving heat transfer, information on transport properties is needed for designing and dimensioning components. These properties appear often in dimensionless numbers such as the Nusselt, Reynolds, Prandtl, Grashof, and Rayleigh numbers.

This paper presents measurements of the thermal diffusivity of R152a which were obtained by dynamic light scattering. The measurements also cover the critical region, where conventional stationary and transient methods for determining thermal diffusivity or conductivity are subject to large errors due to convective effects and are, hence, particularly scarce.

2. MEASUREMENT METHOD

Dynamic light scattering represents a noninvasive optical technique for measuring the thermal diffusivity. The fluid under investigation is kept in thermal equilibrium, with no internal sources of heat or macroscopic temperature gradients present, which is a significant advantage over the conventional techniques of determining transport properties such as the parallel-plate or hot-wire methods [1].

The information on thermal diffusivity is obtained by investigating the relaxation behavior of microscopic thermodynamic fluctuations. Since the method is intrinsically absolute in nature, there is no need for calibration or for introducing correction terms. According to the optical arrangement for detecting the scattered light, measurements can be made in the fluid region (heterodyne detection) and in the extended critical region (homodyne detection) with an uncertainty typically under 2% depending on the investigated region of state. At lower fluid densities (below $100\ \mathrm{kg \cdot m^{-3}}$) the scattered intensities are too low to be evaluated accurately, thus limiting the range of application. For an explicit treatment of dynamic light scattering and its applications we refer to the literature [1–4].

The experimental apparatus used in our investigation has been described in detail in previous publications [5–8]. An argon-ion laser with a maximum power output of 300 mW is focused into a test cell. The light scattered by the microscopic temperature fluctuations is recorded at

variable scattering angles (3–15°) by a photomultiplier. This signal is then fed into a digital correlator which yields the dynamic correlation function $g(t)$, the statistical average behavior of the dissipative fluctuations. A regressional analysis yields the characteristic decay time t_c of this exponential function which determines the thermal diffusivity.

Because of the relatively high critical temperatures of the alternative refrigerants, we have developed an electronically regulated test cell capable of sustaining a long-term temperature stability (± 2 mK over 24 h) at temperatures up to 450 K [9]. This stability is important when measuring in the critical region where the thermal diffusivity a decreases over several orders of magnitude and where macroscopic temperature stability not only limits the possible approach to the critical point, but also represents an increasing source of error in the determination of a. In this investigation we have been able to measure thermal diffusivities to within 0.01 K of the critical point. While the above-mentioned temperature stability would allow for a closer approach, other limiting factors such as multiple scattering, gravity, laser heating, and wavelengths of the fluctuations become major sources of error in this region.

In the extended critical region, measurements were made with the homodyne method of light scattering. The scattered light $\bar{I}_s$ is directly measured by a photomultiplier at angles θ between 8 and 10°. Light scattered off the cell windows I_0 (representing a local oscillator) is effectively screened out of the detection by means of a pinhole situated in front of the cell windows, ensuring the criterion $I \gg \bar{I}_0$ for the evaluation of the correlation function in terms of a single exponential.

In the liquid region, where scattered light intensities are small, the heterodyne method was employed. Here, signal enhancement is achieved by superimposing a local oscillator, i.e., the light I_0 scattered off the cell windows, with I_s. By measuring at small scattering angles (θ between 3 and 5°) and shifting the scattering volume with respect to the window surface, the criterion $I_0 \gg \bar{I}_s$ can be satisfied.

3. RESULTS

The objective behind this investigation was the systematic coverage of a broad region of state within the limits set by the applicability of the method or the apparatus. For this reason, thermal diffusivity measurements were made along four super- and three subcritical isotherms, namely, at $\tau = \pm 10^{-1}$, $\pm 10^{-2}$, $\pm 5 \times 10^{-2}$, and $+10^{-1}$, where τ denotes the reduced temperature difference $(T - T_c)T_c$. Measurements were also made along the critical isochore as well as in both coexisting phases (Table I). On

Table I. Experimental Results for R152a

T (K)	p (MPa)	n	ρ (kg·m^{-3})	$a \times 10^9$ (m^2·s^{-1})
		R152a Isotherms		
367.15	9.35	1.2006	751.8	60.451
367.16	6.36	1.1923	722.2	53.664
367.16	5.12	1.1877	705.6	44.084
367.16	4.11	1.1829	688.3	41.833
367.15	3.17	1.1767	666.1	39.540
367.15	3.09	1.1760	663.6	37.942
367.15	3.09	1.0313	121.5	76.625
367.16	3.07	1.0303	117.6	81.302
367.15	2.79	1.0247	95.9	117.581
367.15	2.52	1.0208	81.1	163.752
367.16	2.23	1.0163	63.4	212.417
382.62	10.72	1.1903	715.1	53.225
382.62	9.74	1.1863	700.4	47.359
382.62	8.38	1.1814	682.9	49.534
382.62	7.31	1.1764	664.9	42.254
382.62	6.57	1.1725	650.7	45.011
382.61	5.92	1.1681	634.8	38.574
382.62	5.28	1.1625	614.7	34.605
382.62	4.91	1.1580	598.2	31.651
382.61	4.62	1.1536	582.1	28.380
382.61	4.39	1.1485	563.2	23.904
382.61	4.20	1.1416	538.2	17.569
382.61	4.17	1.1397	530.9	14.365
382.61	4.17	1.0576	222.7	18.042
382.61	4.11	1.0517	200.3	30.116
382.61	4.04	1.0464	179.7	40.658
382.61	3.95	1.0427	−65.6	50.908
382.61	3.82	1.0383	148.6	64.821
382.61	3.65	1.0343	133.0	80.006
382.61	3.41	1.0295	114.6	101.919
382.61	3.07	1.0240	93.5	134.452
382.61	2.61	1.0182	71.1	191.882
386.10	10.62	1.1868	702.2	55.630
386.10	9.27	1.1808	680.7	49.656
386.09	8.02	1.1757	662.4	43.865
386.09	6.88	1.1693	639.3	36.959
386.09	6.12	1.1636	618.5	34.573
386.09	5.55	1.1576	596.7	31.939
386.09	5.17	1.1524	577.7	29.277

Table I. *(Continued)*

T (K)	p (MPa)	n	ρ (kg·m^{-3})	$a \times 10^9$ (m^2·s^{-1})
386.09	4.86	1.1459	553.9	25.700
386.09	4.67	1.1400	532.0	20.481
386.09	4.56	1.1342	510.8	15.476
386.09	4.49	1.1280	487.7	10.326
386.09	4.46	1.1219	465.2	5.894
386.09	4.45	1.1151	440.0	2.326
386.09	4.45	1.0771	297.1	2.502
386.09	4.45	1.0746	287.5	4.205
386.09	4.44	1.0680	262.4	9.335
386.09	4.41	1.0623	240.5	15.242
386.09	4.36	1.0568	219.7	23.270
386.09	4.30	1.0526	203.7	31.500
386.09	4.19	1.0473	183.1	44.360
386.09	4.03	1.0412	160.0	60.104
386.09	3.82	1.0360	139.6	77.787
386.09	3.55	1.0306	118.8	112.565
386.09	3.26	1.0257	99.8	145.567
386.85	10.53	1.1848	695.1	52.770
386.86	8.92	1.1786	672.9	50.845
386.86	7.77	1.1735	653.3	46.717
386.86	6.74	1.1670	630.8	42.849
386.86	6.12	1.1620	612.6	38.776
386.86	5.62	1.1565	592.6	35.893
386.86	5.25	1.1512	573.1	29.781
386.86	4.96	1.1451	551.0	25.579
386.86	4.81	1.1406	534.2	21.534
386.86	4.67	1.1339	509.7	16.057
386.86	4.61	1.1289	491.1	12.251
386.86	4.56	1.1231	469.5	8.203
386.86	4.55	1.1181	450.9	5.390
386.86	4.54	1.1121	428.9	2.940
386.86	4.53	1.1089	416.8	2.077
386.86	4.53	1.1051	402.4	1.350
386.86	4.53	1.1022	391.5	1.078
386.86	4.53	1.0971	372.4	0.904
386.86	4.53	1.0959	368.1	0.915
386.86	4.53	1.0926	355.7	1.037
386.86	4.53	1.0890	342.2	1.326
386.86	4.53	1.0864	332.4	1.691
386.86	4.53	1.0831	319.9	2.390
386.86	4.51	1.0802	308.7	3.148

Table I. *(Continued)*

T (K)	p (MPa)	n	ρ ($kg \cdot m^{-3}$)	$a \times 10^9$ ($m^2 \cdot s^{-1}$)
386.86	4.51	1.0748	288.5	5.266
386.86	4.49	1.0696	268.3	8.422
386.86	4.49	1.0677	162.2	10.498
386.86	4.45	1.0617	238.4	15.951
386.86	4.40	1.0565	218.6	24.520
386.86	4.32	1.0518	200.3	31.420
386.86	4.21	1.0463	179.5	43.643
386.86	4.04	1.0408	158.3	65.214
386.86	3.86	1.0364	141.2	77.648
386.86	3.57	1.0305	118.7	99.927
386.86	3.25	1.0258	100.5	132.223
386.86	2.93	1.0215	83.8	158.093
386.86	2.45	1.0165	64.5	220.789
390.34	10.42	1.1807	680.4	52.669
390.34	8.92	1.1746	658.3	48.697
390.34	7.98	1.1697	640.5	44.122
390.34	7.14	1.1641	620.5	40.693
390.34	6.50	1.1587	600.5	37.499
390.34	6.03	1.1532	580.5	34.745
390.34	5.81	1.1498	568.2	31.638
390.34	5.56	1.1458	553.4	28.418
390.34	5.33	1.1404	533.4	24.726
390.34	5.17	1.1349	513.2	21.108
390.34	5.07	1.1303	496.4	17.732
390.34	5.00	1.1255	478.4	14.909
390.34	4.94	1.1204	459.7	12.032
390.34	4.90	1.1153	440.6	9.862
390.34	4.88	1.1117	427.3	8.552
390.34	4.86	1.1067	408.5	7.136
390.34	4.85	1.1026	393.3	6.568
390.34	4.84	1.0989	379.4	6.226
390.34	4.83	1.0960	368.5	6.178
390.34	4.82	1.0928	356.3	6.253
390.34	4.81	1.0881	338.5	6.857
390.34	4.79	1.0823	316.6	8.236
390.34	4.77	1.0782	301.1	9.923
390.33	4.74	1.0730	281.4	12.723
390.34	4.71	1.0682	263.2	16.326
390.34	4.66	1.0624	240.9	22.209
390.34	4.59	1.0574	222.0	29.765
390.34	4.51	1.0528	204.2	37.289

Table I. *(Continued)*

T (K)	p (MPa)	n	ρ (kg · m^{-3})	$a \times 10^9$ (m^2 · s^{-1})
390.34	4.37	1.0473	183.2	49.705
390.34	4.21	1.0422	163.6	62.078
390.34	3.97	1.0364	141.2	83.988
390.34	3.65	1.0304	118.2	110.108
390.34	3.43	1.0269	104.7	132.341
390.34	3.06	1.0222	86.6	173.145
390.34	2.55	1.0169	65.9	250.976
405.80	8.97	1.1525	578.1	36.675
405.80	8.17	1.1449	550.3	33.662
405.80	7.72	1.1394	429.8	32.198
405.80	7.46	1.1354	515.2	31.060
405.80	7.05	1.1276	486.2	28.111
405.80	6.80	1.1213	462.9	26.834
405.80	6.63	1.1157	442.0	25.185
405.80	6.48	1.1101	421.2	24.044
405.80	6.39	1.1059	405.4	23.690
405.80	6.28	1.1008	386.4	23.033
405.80	6.18	1.0955	366.7	23.170
405.80	6.14	–.0930	357.1	23.556
405.80	6.06	1.0888	341.3	23.966
405.80	5.98	1.0849	326.4	25.197
405.80	5.88	1.0790	304.3	27.572
405.80	5.78	1.0739	285.0	30.600
405.80	5.68	1.0702	270.6	35.038
405.80	5.47	1.0623	240.6	41.988
405.80	5.39	1.0580	224.3	45.975
405.80	5.22	1.0529	204.7	53.217
405.80	5.08	1.0491	190.3	62.509
405.80	4.89	1.0450	174.6	74.071
405.80	4.65	1.0399	154.9	89.671
405.80	4.41	1.0361	140.3	107.237
405.80	4.08	1.0314	122.1	127.023
405.80	3.70	1.0267	103.7	152.146
405.80	3.40	1.0231	89.7	184.376
425.11	10.37	1.1347	512.7	41.917
425.12	9.73	1.1274	485.8	40.315
425.12	9.41	1.1235	471.3	38.910
425.12	9.01	1.1178	449.9	37.637
425.12	8.71	1.1125	430.0	37.712
425.12	8.43	1.1071	410.1	36.901
425.12	8.20	1.1025	392.9	36.484

Table I. *(Continued)*

T (K)	p (MPa)	n	ρ (kg·m^{-3})	$a \times 10^9$ (m^2·s^{-1})
325.12	7.94	1.0966	370.7	37.327
425.12	7.77	1.0925	355.0	38.529
425.12	7.57	1.0876	336.6	39.412
425.12	7.37	1.0823	316.8	40.796
425.12	7.15	1.0768	296.0	43.226
425.12	6.93	1.0713	275.0	47.129
425.12	6.74	1.0667	257.4	52.247
425.12	6.50	1.0612	236.4	57.703
425.12	6.18	1.0548	211.9	66.518
425.12	5.84	1.0489	189.3	78.706
425.12	5.48	1.0433	167.8	91.631
425.12	5.10	1.0380	147.6	102.962
425.12	4.68	1.0329	127.7	139.392
425.12	4.12	1.0269	104.5	166.032
		R152a 2-phase liquid		
293.15	0.50	1.2473	916.1	66.549
294.86	0.53	1.2458	910.9	68.052
298.15	0.58	1.2436	903.2	66.276
303.15	0.68	1.2402	891.2	64.938
308.15	0.78	1.2363	877.6	61.825
313.16	0.90	1.2325	864.3	62.384
318.16	1.02	1.2284	849.9	59.983
323.16	1.16	1.2240	834.7	58.124
328.16	1.32	1.2199	820.2	56.943
333.16	1.49	1.2152	803.5	56.365
338.16	1.67	1.2108	788.0	54.295
343.16	1.87	1.2058	770.3	52.465
343.16	1.87	1.2058	770.3	53.329
348.16	2.09	1.2005	751.4	52.023
348.16	2.09	1.2005	751.4	51.700
353.16	2.33	1.1945	730.2	49.353
353.16	2.33	1.1945	730.2	48.664
358.16	2.58	1.1884	708.1	45.189
358.16	2.58	1.1884	708.1	46.859
363.15	2.86	–	–	41.750
363.16	2.86	1.1816	683.8	43.251
366.05	3.04	1.1774	668.4	39.143
370.65	3.33	1.1698	641.0	33.763
374.22	3.56	1.1628	615.5	30.439
376.98	3.76	1.1569	594.1	26.081
379.11	3.91	1.1511	572.9	22.389

Table I. *(Continued)*

T (K)	p (MPa)	n	ρ (kg · m^{-3})	$a \times 10^9$ (m^2 · s^{-1})
380.77	4.04	1.1463	555.4	18.943
382.05	4.14	1.1417	538.5	14.867
383.04	4.22	1.1379	524.5	13.084
383.81	4.28	1.1343	511.1	10.914
384.40	4.32	1.1310	498.8	9.274
384.86	4.36	1.1280	487.9	7.517
385.22	4.39	1.1252	477.6	6.177
385.49	4.41	1.1228	468.5	5.162
385.71	4.43	1.1207	460.9	4.166
385.88	4.44	1.1184	452.3	3.325
386.00	4.46	1.1170	447.1	2.680
386.11	4.46	1.1152	440.2	2.187
386.19	4.47	1.1138	435.1	1.806
386.25	4.48	1.1120	428.3	1.397
386.30	4.48	1.1109	323.1	1.129
386.34	4.48	1.1098	420.2	0.950
386.36	4.49	1.1083	414.4	0.746
386.39	4.49	1.1074	411.3	0.602
386.41	4.49	1.1070	409.8	0.555
386.43	4.49	1.1055	404.0	0.390
386.44	4.49	1.1045	400.1	0.293
386.45	4.49	1.1032	395.3	0.212
386.46	4.49	—	—	0.157
		R152a 2-phase vapor		
348.16	2.09	1.0186	72.3	141.919
353.16	2.33	1.0210	81.6	114.263
358.16	2.58	1.0241	93.8	107.563
363.16	2.86	1.0277	107.8	88.385
366.05	3.04	1.0304	118.0	78.510
370.65	3.33	1.0347	134.9	63.814
374.22	3.56	1.0389	151.1	50.776
376.98	3.76	1.0437	169.3	39.434
379.11	3.91	1.0473	183.1	31.230
380.77	4.04	1.0511	197.8	24.806
382.04	4.14	1.0543	210.1	19.627
383.04	4.21	1.0578	223.4	15.726
383.81	4.27	1.0610	235.9	12.458
384.40	4.32	1.0632	244.1	10.063
384.86	4.36	1.0662	255.7	7.968
385.22	4.39	1.0684	264.1	6.291
385.49	4.41	1.0710	273.7	5.016

Table I. *(Continued)*

T (K)	p (MPa)	n	ρ (kg·m^{-3})	$a \times 10^9$ (m^2·s^{-1})
385.71	4.43	1.0727	280.2	4.179
385.87	4.44	1.0745	287.0	3.392
386.00	4.46	1.0764	294.2	2.725
386.11	4.46	1.0781	300.7	2.211
386.19	4.47	1.0794	305.8	1.872
386.25	4.48	1.0806	310.1	1.492
386.30	4.48	1.0823	316.9	1.204
386.33	4.48	1.0834	320.7	0.991
386.37	4.49	1.0843	324.4	0.786
386.39	4.49	1.0852	327.6	0.623
386.41	4.49	1.0860	330.7	0.587
386.43	4.49	1.0871	334.8	0.399
386.44	4.49	1.0877	337.3	0.302
		R152a critical isochore		
386.53	4.50	1.0971	372.6	0.212
386.54	4.50	1.0971	372.6	0.273
386.56	4.50	1.0971	372.6	0.317
386.58	4.50	1.0971	372.6	0.375
386.62	4.51	1.0972	372.8	0.421
386.66	4.51	1.0971	372.6	0.534
386.71	4.51	1.0971	372.6	0.642
386.78	4.52	1.0960	368.6	0.776
386.87	4.53	1.0955	366.4	0.916
386.99	4.54	1.0955	366.4	1.146
387.14	4.55	1.0954	366.2	1.390
387.34	4.57	1.0954	366.2	1.731
387.59	4.59	1.0954	366.2	2.137
387.91	4.62	1.0954	366.2	2.615
388.33	4.65	1.0954	366.2	3.305
388.87	4.70	1.0949	364.3	4.073
389.57	4.76	1.0949	364.7	5.086
390.47	4.83	1.0949	364.7	6.252
391.64	4.93	1.0949	364.7	7.679
393.15	5.06	1.0949	364.7	9.957
395.09	5.23	1.0949	364.7	12.462
397.61	5.44	1.0949	364.7	15.437
400.85	5.72	1.0949	364.7	18.855
405.04	6.08	1.0949	364.7	22.790
410.45	6.52	1.0949	364.7	28.276
417.45	7.12	1.0949	364.7	33.516
426.48	7.88	1.0949	364.7	41.487

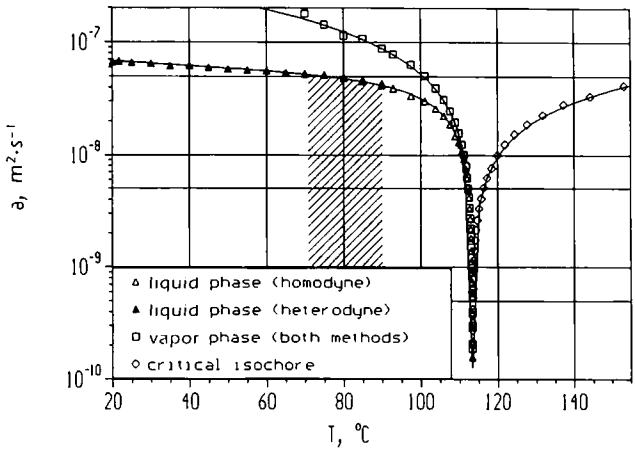

Fig. 1. The thermal diffusivity a of R152a as a function of temperature along the critical isochore above the temperature and on the coexisting vapor and liquid branches below the critical temperature.

average, 35 measurement points were taken along each path. The covered region of state expressed in terms of density and pressure is approximately $100\ \text{kg} \cdot \text{m}^{-3} < \rho < 1200\ \text{kg} \cdot \text{m}^{-3}$ and $290\ \text{K} < T < 420\ \text{K}$. While the measurements at higher temperatures and pressures were restricted by the pressure resistance of the quartz cell windows, those obtained in the

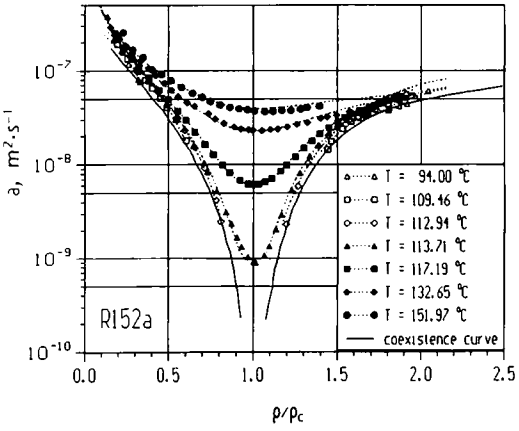

Fig. 2. The thermal diffusivity a of R152a as a function of the reduced density ρ/ρ_c.

low-density region were limited by the applicability of the method due to low light-scattering intensities.

In addition to the thermal diffusivity, the temperature, pressure, and refractive index of the substances were also measured. With the aid of the Lorentz–Lorenz relation, density values can be calculated from the refractive-index measurements. Figures 1 and 2 show the measured values of thermal diffusivity a of R152a. Figure 1 shows a as a function of temperature for both coexisting phases and for the critical isochore. At temperatures below 90°C, the heterodyne technique was applied, while the other regions were investigated with the homodyne technique of light scattering. The region of overlap $70°C \leqslant T \leqslant 90°C$ shows good agreement between the two methods. As can be seen from Fig. 1, the combination of the two techniques allows for a wide range of states to be investigated. The semilogarithmic presentation in Fig. 2 depicts a against the reduced density ρ/ρ_c in the coexisting vapor and liquid phases and along seven isotherms.

6. ACCURACY

6.1. Thermal Diffusivity

Since dynamic light scattering represents a statistical process, the measurements of diffusivities are invariably subject to statistical deviations in addition to experimental errors. In the following we briefly classify the main sources of error. The equation determining the thermal diffusivity can be

$$a = \frac{1}{t_c q^2} \tag{1}$$

expressed as [1–4], where q is the scattering vector and defines the scattering geometry:

$$|\vec{q}| = q = \frac{4\pi n}{\lambda_L} \sin\left(\frac{\theta}{2}\right) \tag{2}$$

Here n is the refractive index of the fluid, λ_L the wavelength of the incident light, and θ the scattering angle. Errors made in the determination of $\vec{q}$ can be easily assessed.

λ_L: The error in the wavelength of the incident light can be neglected, as the use of a frequency stabilizing etalon reduces this error to the order of 0.001%.

n: Aside from its direct influence on a, refractive-index errors also affect the determination of the scattering angle θ due to the optical geometry. However, both errors have a compensating effect, such that a deviation $\Delta n/n$ of 10% contributes an error in $\Delta a/a$ of only 0.3% [8]. Thus measurements of the refractive index need not necessarily be made. In our experiments the refractive index is determined with an uncertainty of $\Delta n < 5 \times 10^{-4}$. The resulting uncertainty in $\Delta a/a$ is of the order of 0.08%.

θ: The scattering angle must be carefully measured. In our apparatus, θ is measured with an accuracy $\Delta\theta < 6$ in with a high precision dividing head. Thus, its overall effect on $\Delta a/a < 0.05\%$ is relatively small.

t_c: The main source of error lies in the determination of the decay time t_c with digital correlation due to the statistical process involved. A detailed treatment of the statistical accuracy in light-scattering experiments, including such error sources as afterpulse and dead-time effects of the detection system, bias, and optimizing experimental parameters (such as photon counts/sample time, sample time/decaytime, run time, etc.), can be found in Refs. 8, 10 and 11.

Perhaps the single largest error in light-scattering experiments arises from an undesired influence of partial heterodyning or homodyning. If the afore-mentioned assumptions $\bar{I}_s \gg I_0$ or $I_0 \gg \bar{I}_s$ are not satisfied in homodyne or heterodyne experiments, respectively, the correlation function, which is fitted to a single exponential, is contaminated by the addition of a second exponential, the decay times differing by a factor 2. An I_0 contribution of 0.5% in homodyne experiments can already account for errors in the determination of a of the order of 1% [12]. $\bar{I}_s/I_0$ can be estimated from the correlated data or obtained directly by experiment (evacuating the test cell, keeping all other parameters constant). In homodyne experiments, this source of error becomes noticeable farther away from the critical point, where low light-scattering signals and a correspondingly high laser power increase the contribution from I_0. We have been able to keep the influence of this error source on a under 1% in most cases.

In the immediate vicinity of the critical point the geometry of the test cell and that of the optical setup increasingly influence the accuracy of diffusivity measurements. Gravity, multiple scattering, and limits imposed by the hydrodynamic theory and laser heating are the main sources of error and have been treated in Ref. 9. The overall uncertainty of our thermal-diffusivity measurements lies between 0.5 and 5%, those obtained in the

critical region being more accurate than measurements made in regions of low light-scattering intensities.

6.2. P, ρ, T Data

T: The fluid temperature was measured with a low-drift platinum resistance thermometer (PT 100) with a resolution under 1 mK. Calibration resulted in a maximum absolute temperature deviation of 20 mK between 50 and 150°C. A repeated measurement of the critical temperature of R22 within 2 years revealed negligible drift.

P: A piezoresistive pressure transducer was used for the measurements. Here calibration over 15 MPa resulted in a maximum deviation of 0.005 MPa while the resolution was under 0.0001 MPa.

ρ: The density was calculated from the refractive-index data through the Lorentz–Lorenz relation. With $\Delta n = 5 \times 10^{-4}$, the resulting uncertainty in the density measurements is 0.3%. A comparison of our measured R22 densities with an accurate equation of state [13] yielded maximum deviations of 0.7%.

5. EVALUATION

5.1. Critical Values

Measurements made along the coexistence curve and the critical isochore near the critical point enable the determination of the critical parameters. The critical temperature T_c is determined by an optical method and by the evaluation of the refractive-index data, the latter method being the more precise. The refractive-index measurements also yield values for n_c and, with ρ_c from the literature, the Lorentz–Lorenz constant LL_c. Table II lists the critical values of R152a. While the critical temperature of

Table II. Critical Parameters of R152a

T_c (K)	n_c	p_c (MPa)	ρ_c (kg · m^{-3})	LL_c (m^3 · kmol^{-1})
386.47	1.0959	4.495	368[a]	11.270

[a] From Ref. 14.

Table III. Coefficients in Eqs. (3) and (4)

Critical isochore		Liquid phase			Vapor phase		
$a_0 \times 10^7$ $(m^2 \cdot s^{-1})$	μ	$a_0 \times 10^7$ $(m^2 \cdot s^{-1})$	μ_0	μ_1	$a_0 \times 10^7$ $(m^2 \cdot s^{-1})$	μ_0	μ_1
2.548	0.807	9.625	0.870	4.11	8.713	0.856	0.68

R152a is in good agreement with the literature value [14], the critical pressure differs significantly.

5.2. Thermal Diffusivity

The thermal-diffusivity data obtained along the coexistence curve and on the critical isochore, when plotted in double-logarithmic form as a function of the reduced temperature, appear as a straight line in the critical region and can be described by a simple power law which is also in accordance with scaling theory:

$$a = a_0 \tau^{\mu} \tag{3}$$

This equation can be used to describe the thermal diffusivity along the critical isochore in the entirely range investigated. However, in the liquid and vapor phases, the measurements deviate from a simple power law farther away from the critical point. As expected, the values in the liquid phase level out to near-linear behavior, while those along the vapor phase increase, reflecting ideal-gas behavior. With the addition of a temperature-dependent term in the exponent, this behavior can be incorporated as

$$a = a_0 |\tau|^{\mu_0 + \mu_1 |\tau|} \tag{4}$$

Table III gives the coefficients of this equation obtained by regressional analysis along the various paths for R152a. The exponents μ and μ_0 are larger than the theoretical value $\nu = 0.63$ from scaling theory [15]. A regional fit of our data approaching the critical point shows no indication of these values to decrease. The data can also be fitted to an expansion,

$$a = a_0 |\tau|^{\mu} (1 + a_1 \tau^{\Delta} + a_2 \tau^{2\Delta} \cdots) \tag{5}$$

in an extended region around the critical point, with Δ being a correction exponent [16]. However, the initial values for μ and Δ have to be kept

within strict boundaries close to the expected theoretical values, and standard deviations of the fit double.

A simple expression for the thermal diffusivity along isotherms as a function of density is more difficult to establish, due to the large differences encountered when describing the values ranging from the ideal-gas region ($a \to \infty$), over the critical point ($a \to 0$) to the liquid region, where a exhibits linear behavior. A comprehensive equation for the thermal diffusivity of R152a representing our measurements has recently been developed by Krauss et al. [17].

6. CONCLUSIONS

Light-scattering measurements of the thermal diffusivity of the alternative refrigerant R152a have been presented. This method is an effective technique for measuring this transport property in a broad range of densities corresponding to $100\ \mathrm{kg \cdot m^{-3}} < \rho < 1200\ \mathrm{kg \cdot m^{-3}}$. By combining the techniques of homodyne and heterodyne detection, measurements can be made up to pressures and temperatures usually limited by constraints imposed by the test cell. In the gas region at lower densities, dynamic light scattering is subject to increasing errors due to low scattering intensities and thus cannot be applied. The uncertainty of the light-scattering measurements varies between 0.5 and 5.0%, depending on the investigated region of state. Near the critical point the measurements can be described by power laws and simple equations within 10%.

ACKNOWLEDGMENTS

The authors would like to express their gratitude to the Deutsche Forschungsgemeinschaft (DFG) for supporting this research project.

REFERENCES

1. W. A. Wakeham, A. Nagashima, and J. V. Sengers (eds.), *Measurement of Transport Properties of Fluids* (Blackwell Scientific, Oxford, 1991).
2. B. J. Berne and R. Pecora, *Dynamic Light Scattering* (Wiley, New York, 1976).
3. B. Chu, *Laser Light Scattering* (Academic, New York, 1974).
4. R. Pecora, *Dynamic Light Scattering, Applications of Photon Correlation Spectroscopy* (Plenum, New York, 1985).
5. E. Reile, P. Jany, and J. Straub, *Wärme-Stoffübertragung* **18**:99 (1984).
6. P. Jany and J. Straub, *Int. J. Thermophys.* **8**:165 (1987).
7. B. Kruppa and J. Straub, *Exp. Therm. Fluid Sci.* **6**:28 (1993).
8. B. Kruppa, *Die temperaturleitfähigkeit alternativer Kältemittel in einem weiten Temperatur- und Dichtebereich*, Ph.D. thesis (Technical University, Munich, 1993).

9. B. Kruppa and J. Straub, *Int. J. Thermophys.* **9**:911 (1988).
10. E. Jakeman, E. R. Pike, and S. Swain, *J. Phys. A* **4**:517 (1971).
11. V. Degiorgio and L. B. Lastovka, *Phys. Rev. A* **4**:2033 (1971).
12. N. C. Ford, *Chem. Scripta* **2**:193 (1972).
13. V. Marx, A. Pruss, and W. Wagner, *Fortschritt- Berichte VDI* **19**:57 (1992).
14. B. Saager and J. Fischer, *Deutscher Kältle Klimatechswischer Verein e. V.* **16**:213 (1989).
15. J. V. Sengers, *Int. J. Thermophys.* **6**:203 (1985).
16. F. J. Wegner, *Phys. Rev. B* **3**:4529 (1972).
17. R. Krauss, V. C. Weiss, T. A. Edison, J. V. Sengers, and K. Stephan, *Int. J. Thermophys.* **17**:731 (1996).